Power, Energy and Electrical Engineering
M. Deng (Ed.)

doi:10.3233/ATDE240345

Design and Optimization of a Low TSR H-Darrieus Turbine Based on Geometry Parameterization Through Joukowsky Transformation

Giusep Baca [a,1], Gabriel Bertacco dos Santos [a] and Leandro Oliveira Salviano [a]
[a] *Faculty of Mechanical Engineering São Paulo State University, Ilha Solteira, SP, Brazil*

Abstract. Amidst the reserves of fossil fuels and surging energy demands, the focus has shifted towards harnessing renewable energy sources like wind energy. This research endeavors to pinpoint the optimal design for a low Tip Speed Ratio (TSR) H-Darrieus turbine at three distinct TSRs: 2.33, 2.64, and 3.09. The study synergizes Computational Fluid Dynamics (CFD) with the Metamodel of Optimal Prognosis (MOP) response surface methodology. The Joukowsky transformation parametrization is applied to symmetrical airfoils, evaluating three pivotal parameters: the a/b ratio, m, and pitch angle. Notably, the pitch angle emerges as the predominant contributor, accounting for over 76% of the effect. Through Gradient-based optimization techniques, the refined turbine design achieved a performance enhancement, peaking at 14.73% for a profile optimized at a TSR of 2.64. Additionally, this work presents an insightful comparison of the non-dimensional velocity and torque coefficients across the considered TSRs. The integration of Ansys Fluent and Ansys OptiSlang in this research affirms a robust, cost-efficient, and fitting approach to dissect fluid dynamics in intricate, computation-intensive CFD models across varying TSRs.

Keywords. H-Darrieus turbine, Computational Fluid Dynamics (CFD), Low Tip Speed Ratio (TSR), Metamodel of Optimal Prognosis (MOP), Pitch angle

1. Introduction

The escalating global energy demand has intensified the exploration for renewable alternatives, with wind energy standing out as a sustainable option. Horizontal Axis Wind Turbines (HAWTs) are predominant in large-scale wind projects due to their efficiency. In contrast, Vertical Axis Wind Turbines (VAWTs), especially H-Darrieus turbines, are optimal for urban areas due to their omnidirectional wind capture and reduced maintenance needs [1-3].

Research has delved into the effects of airfoil thickness and the position of maximum thickness on H-Darrieus turbines, suggesting the potential of the Joukowsky transformation as an efficient optimization method [4-6]. Challenges like dynamic stall at low Tip Speed Ratios (TSR) can be mitigated through optimized blade pitching [7-9]. While enhancing aerodynamic performance is crucial, detailed studies often resort to simplified methods due to computational constraints. The Metamodel of Optimal Prognosis (MOP) offers a solution by reducing computational overhead, and it's pivotal

[1] Corresponding Author, Giusep Baca, Faculty of Mechanical Engineering São Paulo State University, Ilha Solteira, SP, Brazil; E-mail: g.bernabe@unesp.br.

for design exploration [10-12]. This study further investigates specific TSRs, employing optimization to determine optimal parameters and contrasting the results with established profiles to determine the most efficient design.

2. H-Darrieus Turbine

The H-Darrieus turbine, a prominent VAWT variant, has blades that undergo varying flow velocities due to changes in the Angle of Attack (AoA) during rotation. The resultant force from lift (F_L) and drag (F_D)provides torque through tangential (F_T) and normal (F_N) components.
The Tip Speed Ratio (TSR), vital for assessing blade AoA, is:

$$\lambda = \frac{w_b R}{U_\infty} \tag{1}$$

Another key metric is solidity (σ):

$$\sigma = \frac{N_b C}{D} \tag{2}$$

Performance of VAWTs is primarily gauged using the instantaneous moment coefficient C_t and the power coefficient C_P:

$$C_t = \frac{M}{\frac{1}{2}\rho A R U^2} \tag{3}$$

$$C_P = \frac{P}{\frac{1}{2}\rho A R U^3} \tag{4}$$

Rotor specs include: 3 blades, 1.03m diameter, NACA 0021 airfoil, and a tip speed ratio of 2.64.

3. CFD Methodology

3.1. Governing Equations

For incompressible and transient flow, the continuity and momentum (Navier–Stokes) equations define the flow field over fluid domains [13-14]. The strain rate (τ_{ij}) is expressed as:

$$\tau_{ij} = \mu\left[\left(\frac{\partial u_i}{\partial x_j} + \frac{\partial u_j}{\partial x_i}\right) - \frac{2}{3}\delta_{ij}\frac{\partial u_j}{\partial x_i}\right] \tag{5}$$

3.2. Turbulence Models

Turbulence models, crucial for wind turbine CFD modeling, are categorized into hybrid models, LES, and RANS. The k-ω model surpasses the standard k-ϵ model for flows with adverse pressure gradients [13,15]. The hybrid Shear Stress Transport (SST) model combines the k-ϵ and k-ω models, being suitable for regions near the walls and fully turbulent flows [16]. Table 1 briefly outlines the simulation settings.

Table 1. Simulation settings

Characteristics	Turbine
Fluid properties	Incompressible
Turbulence model	k-ω SST
Maximum residuals	1e-06
Solver	Pressure based
Turbulent Kinetic Energy	Second Order Upwind
Specific Dissipation Rate	Second Order Upwind
Pressure-Velocity solution	Coupled

3.3. Fluid Domain

The performance of a low TSR H-Darrieus turbine is studied at a free stream velocity (refer to Figure 1). The computational domain's dimensions adhere to established guidelines [4], and the boundary conditions are defined based on the domain's inner diameter D.

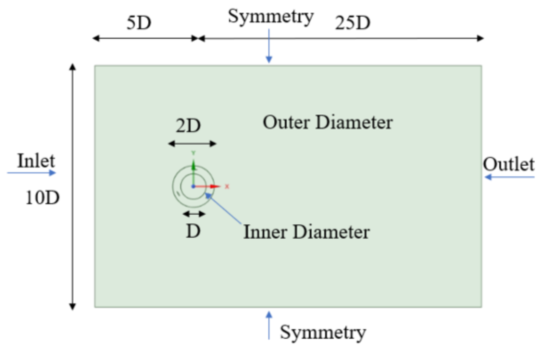

Figure 1. Computational domain dimensions in function of D.

3.4. Computational Mesh

An unstructured mesh was used for the 2-D H-Darrieus turbine due to its adaptability to complex geometries. The mesh around the NACA 0021 profile features 30 layers with specific characteristics. Mesh quality metrics, including orthogonal quality and skewness, were assessed (see Table 2). The entire computational modeling involved 285 geometry samples using Ansys software.

Table 2. Meshing metrics

Orthogonal quality		Skewness	
Minimum	0.11345	**Minimum**	2.1423e-02

Maximum	0.99457	**Maximum**	0.98231
Average	0.95897	**Average**	1.1134e-2
Standard deviation	5.345e-2	**Standard deviation**	2.035e-2

3.5. Revolution Analysis

For the reference scenario (NACA 0021, TSR=2.64), 90 revolutions were simulated (Figure 2.a). Results indicate a change in average Cp below 0.28% after 20 revolutions, which is in line with findings by Balduzzi and Lam et al. [17-18], but more stringent than Trivellato et al. [19].

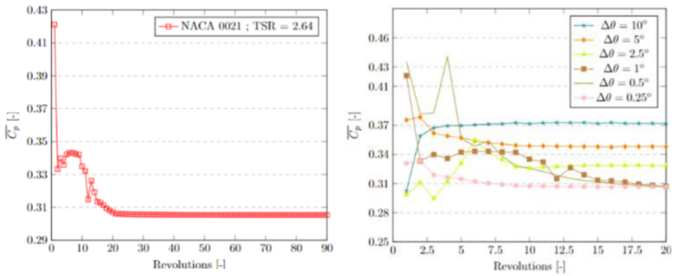

Figure 2. a) Average Cp vs Revolutions, b) Average Cp vs Azimuthal increment

3.6. Azimuthal Increment Analysis

Figure 2.b showcases the relationship between average Cp and turbine revolution for various azimuth angles ($\Delta\theta$). Simulations with $\Delta\theta$ values of 10° and 5° were less accurate, while $\Delta\theta$ of 2.5° overestimated average Cp. $\Delta\theta$ = 1° emerges as the optimal choice for the given TSR at moderate flow conditions [20].

3.7. Grid Convergence Analysis

The NACA 0021 airfoil was evaluated with three mesh types: refined, medium, and coarse. Using the Grid Convergence Index (GCI) approach by Celik, the discretization error was assessed [21]. Simulations were conducted, and the average power coefficient values were found for each mesh. The error for the medium mesh was 0.1903%, making it suitable for CFD simulations with limited uncertainty.

3.8. Validation Study

The research validates a 3-bladed H-Darrieus turbine with a NACA 0021 airfoil (Table 1) at TSRs of 1.44 to 3.29 and a free stream velocity of 9 m/s. Using a 6.3% turbulent intensity at the inlet, based on findings from Belabes et al. [22], the results closely align with experimental data from Castelli et al. [23]

Figure 3 compares the turbine's average Cp from CFD results to the experimental data from Castelli et al. [23].

4. Methodology for Parameter Optimization Through the Metamodel of Optimal Prognosis

This chapter elaborates on the optimization of VAWTs using input parameter identification, Design of Experiments (DoE), and the Metamodel of Optimal Prognosis (MOP). The methodology is summarized in Figure 4.

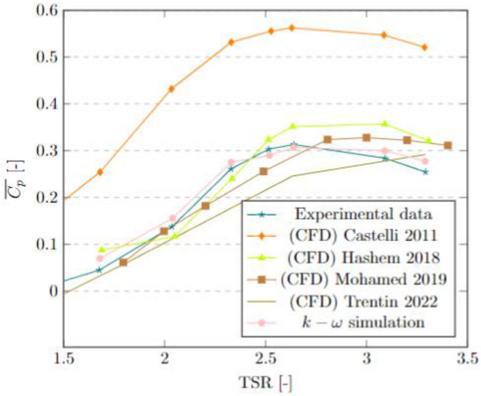

Figure 3. Comparison of experimental and numerical validation results

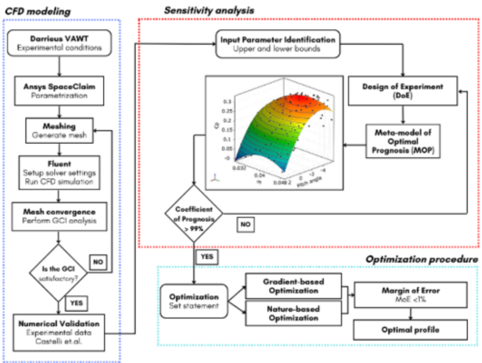

Figure 4. CFD modeling, Sensitivity Analysis, and Optimization

4.1. Input Parameter Identification

4.1.1. Geometry Parameterization via Joukowsky Transformation

The Joukowsky transformation is used to convert a circle into an airfoil shape in the complex plane. According to the established method in Zhang et al. [24], the airfoil's parametric equation for a symmetric profile is:

$$\Omega = \sqrt{\left(a\cos(\theta)\right)^2 + \left(b\sin(\theta)\right)^2} \tag{6}$$

$$X = \left[\Omega + \frac{\left(\frac{C_J}{2}\right)^2}{\Omega}\right] \cos(\alpha)\,, \alpha \in [0,2\pi] \tag{7}$$

$$Y = \left[\Omega - \frac{\left(\frac{C_J}{2}\right)^2}{\Omega}\right] \sin(\alpha)\,, \alpha \in [0,2\pi] \tag{8}$$

$$\alpha = \pi - arccos\left(\frac{m - acos(\theta)}{\Omega}\right), \alpha \in [0,2\pi] \tag{9}$$

Where the ratio *a/b* controls the position of maximum thickness of the profile and *m* control the profile's relative thickness.

4.1.2. Pitch Angle

The pitch angle significantly impacts VAWT performance. Various studies, such as Klimas et al. [25] and Rezaeiha et al. [9], have highlighted its importance. Given its influence on efficiency, the pitch angle is chosen as a key parameter for optimization. Some Common Mistakes

4.2. Metamodel of Optimal Prognosis (MOP)

Meta-modeling [10] is pivotal in design exploration, particularly when navigating intricate or computationally intensive physical models. The MOP serves as a bridge, offering surrogate models that streamline these complexities. Central to its efficacy are several key coefficients:

- **Coefficient of Determination (CoD)**: This coefficient quantifies the precision of a polynomial regression model, emphasizing the fraction of variability accounted for by the approximation [11].

- **Coefficient of Importance (CoI)**: Pioneered by [12], the CoI assesses the relevance of an input variable by juxtaposing the CoD of the holistic and pared-down models.

- **Coefficient of Prognosis (CoP)**: Crafted as a model-agnostic metric, the CoP [11] is instrumental in ascertaining the caliber of meta-models.

Leveraging these coefficients, the MOP meticulously evaluates response surfaces, which are sculpted through diverse techniques:

- **Polynomial Regression**: This approach, used for model response approximation, involves polynomial basis functions, defining the relation between model output and approximation value.

- **Moving Least Squares (MLS)**: MLS uses variable coefficients in contrast to global polynomial regression coefficients.

- **Kriging Approximation**: Kriging, known for its reliability in forecasting, models Gaussian spatial variations and is popular in optimization.

4.3. Optimization Statement

CFD inputs are derived from the pitch angle (β) and geometry parameterization, specifically the shifted distance (m) and the major-minor axis ratio (a/b). The ratio (a/b) influences maximum thickness positioning, while *m* dictates relative thickness. Based on the characteristics of the NACA 0021 airfoil and previous H-Darrieus turbine studies [20, 25], the input boundaries are shown in Table 3:

Table 3. Lower bound and upper bound for the variables

Input variable	Lower bound	Upper bound
(a/b)	0.95	1.09
m	0.03	0.053
β	-7	4

In analyzing VAWT performance across specific TSR values, various analytical methods are employed. One prominent approach is gradient-based optimization. Newton's method, derived from derivative computations, is adapted when the CAE solution remains unclear. The Nonlinear Programming by Quadratic Langrangian (NLPQL) is efficient for scenarios with fewer design variables but leans on alternative strategies as complexity increases [26]. Another method, the Downhill Simplex (Simplex), is iterative, adjusting based on target function values [27].

The overarching objective is articulated as:

$$\text{Find } X = \left\{\frac{a}{b}, m, \beta\right\}^T \text{ that maximizes the average } C_p.$$

4.4. Margin of Error

CFD simulations validate optimal control points from gradient-based models. Model outputs are gauged by the Margin of Error (MoE), calculated as:

$$\left|\frac{Z - Z_i}{Z}\right| = MoE \tag{10}$$

where Z is the CFD simulation result and Z_i is the optimization model predicted output. Outputs with an MoE below 1% are deemed reliable; those exceeding this are discarded. The optimal profile is then shaped using the top-performing model, with selections anchored in the computational validation of the average Cp value.

5. Results

5.1. Response Surfaces Assessment

After conducting CFD simulations using Ansys Fluent for LHS-based design point sampling, meta-models were developed for different TSRs, including Linear Regression Models, Moving Least Squares, and Kriging. Among these, the Linear Regression Model

of order 2 was identified as the most fitting for various TSRs based on the Coefficient of Determination (CoD) and Coefficient of Prognosis (CoP).
3D heat maps (Figure 5 and 6) were created for each TSR, plotting the pitch angle (β), relative thickness (m), and position of maximum thickness (a/b) against the average *Cp*. The zone of maximum average *Cp* is discerned as a peak region.

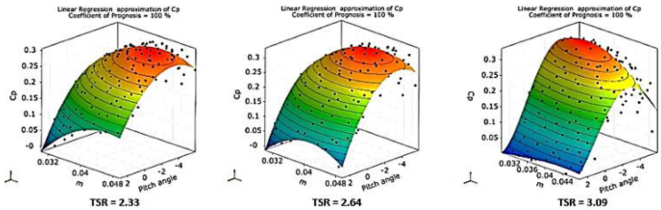

Figure 5. 3D surfaces for each TSR plot pitch angle (β), relative thickness (m), and average Cp

Analyzing the CoI matrix, significant insights were derived:

- At TSR = 2.33, the pitch angle *β* had the most substantial contribution at 76%, followed by the relative thickness *m* at 18.9% and the position of maximum thickness (a/b) at 5.1%.

- With increasing TSR values, the contribution of *β* and (a/b) saw an upswing, while the contribution of *m* showed a decline.

- These trends mirror the findings of Trentin et al. [36], underscoring the pivotal role of pitch angle *β* in enhancing the average *Cp* of VAWTs.

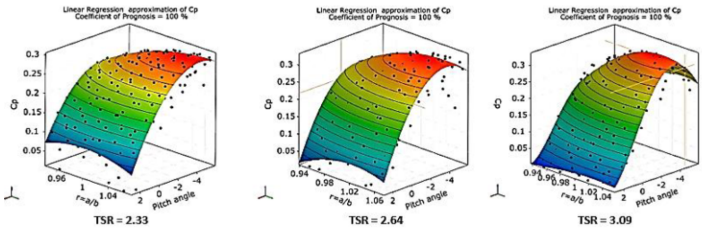

Figure 6. 3D surfaces for each TSR map pitch angle (β), maximum thickness (a/b), and average Cp.

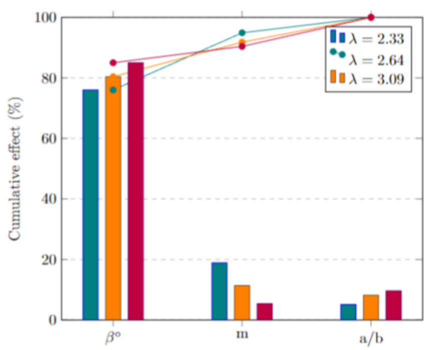

Figure 7. CoI at different TSR

5.2. Optimization Process and Outcomes

Utilizing gradient-based optimization techniques, optimal input parameters (a/b, m, β) for maximum average Cp were identified for each TSR. Both SIMPLEX and NLPQL methods were employed, achieving a coefficient of prognosis above 99%. Validations were made through CFD simulations ensuring a margin of error below 1%.

Table 4 presents the summarized optimum designs and performance specifics for each TSR. For instance, at TSR = 2.33, optimal values are: a/b=1.028, m=0.0447, and β=−3.940°, leading to an average Cp increase of 11.47%.

Table 4. Summary of optimum design points

TSR	Optimization	Optimal $\frac{a}{b}$	Optimal m	Optimal β	C_p Incr.
2.33	SIMPLEX	1.028	0.0447	-3.940	11.47%
2.64	NLPQL	1.047	0.0417	-3.613	14.73%
3.09	SIMPLEX	1.066	0.0388	-3.271	13.39%

Figure 8 contrasts the NACA 0021 profile with optimal profiles across different TSRs. As TSR rises, the location of maximum thickness (a/b) increases, while relative thickness (m) decreases. Pitch angle, β, also shows variation with TSR.

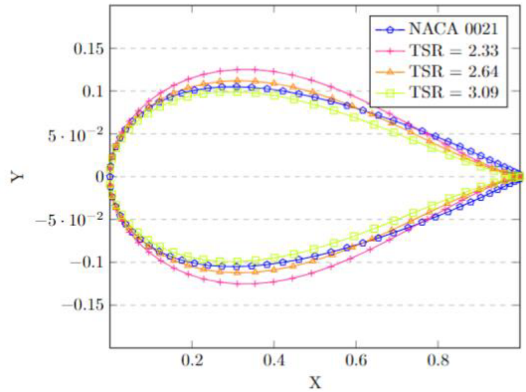

Figure 8. NACA 0021 profile with optimal profiles across different TSRs.

5.3. Comparative Analysis of Optimal Profiles at Different TSRs

5.3.1. Torque Coefficient

TSR = 2.33: The optimal profile shows a lower negative torque coefficient range than the NACA 0021 profile (Figure 9.a).

TSR = 2.64: The optimal profile doesn't exhibit negative torque coefficients in three regions of its rotation, outperforming the NACA 0021(Figure 9.b).

TSR = 3.09: Both optimal and NACA 0021 profiles have no negative torque coefficients (Figure 9.c).

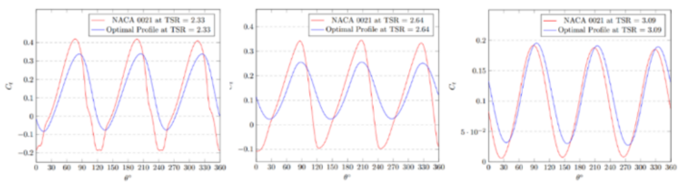

Figure 9. a) C_t comparison at TSR = 2.33, b) C_t comparison at TSR = 2.64, c) C_t comparison at TSR = 3.09.

5.3.2. Aerodynamic Performance:

TSR = 2.33: The optimized configuration demonstrates improved performance with higher minimum torque coefficient and lacks drag zones causing flow separation seen in NACA 0021 (Figure 10).

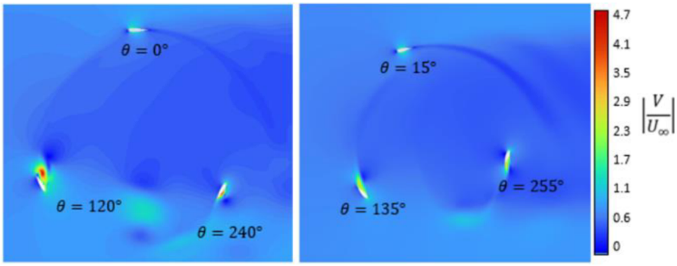

a) b)

Figure 10. Dimensionless velocity contour for a) NACA 0021 and b) the optimal profile at TSR = 2.33.

TSR = 2.64: The optimal profile indicates smoother flow with no drag zones, enhancing aerodynamic performance (Figure 11).

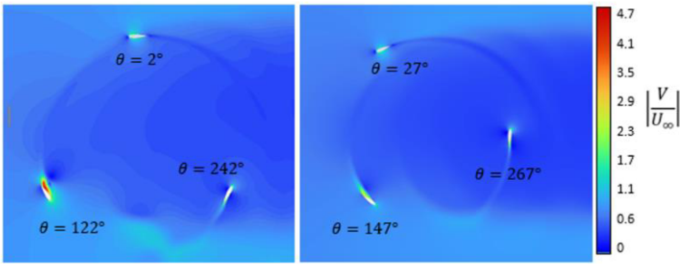

a) b)

Figure 11. Dimensionless velocity contour for a) NACA 0021 and b) the optimal profile at TSR = 2.64.

TSR = 3.09: Both profiles exhibit smooth flow patterns, leading to the absence of negative torque coefficient values (Figure 12).

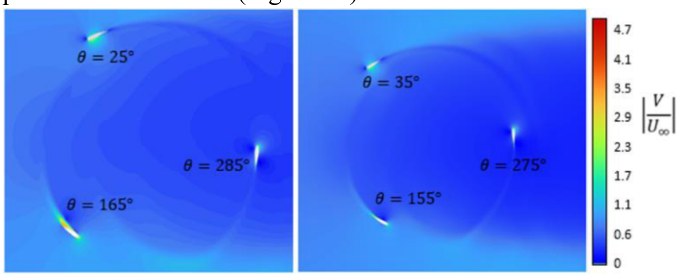

a) b)

Figure 12. Dimensionless velocity contour for a) NACA 0021 and b) the optimal profile at TSR = 2.64.

H-Darrieus turbine has three optimal profiles tailored for specific TSRs, each with distinct performance across TSR ranges (Figure 13). Specifically:

- The TSR=2.33 profile excels at lower TSRs but lags at higher ones.

- The TSR=3.09 profile dominates at higher TSRs but underperforms at lower ones.

- The TSR=2.64 profile, though not peak at extremes, maintains balanced performance, making it the most versatile for varied TSRs.

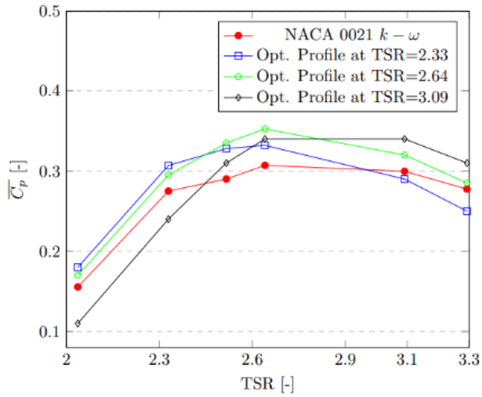

Figure 13. Comparison between the NACA 0021 and the three optimized profiles.

6. Conclusions

The study optimized a low TSR Darrieus turbine across TSRs 2.33, 2.64, and 3.09, analyzing the role of maximum thickness position (a/b), relative thickness (m), and pitch angle (β).
Key Insights:

- Model Selection: The second-order linear regression was the most suitable model for all TSRs.

- Sensitivity Analysis: Among the parameters, pitch angle (β) dominated with a contribution over 76%, followed by (m) and (a/b). This aligns with Trentin et al. [28]'s emphasis on the pitch angle's significance in VAWT.

- Optimal Inputs: With increasing TSR, both the ideal (a/b) and pitch angle (β) rise, while the ideal (m) falls. These results guide Darrieus turbine design optimization.

- Performance Comparison: Among the profiles, the one optimized for TSR=2.64 stands out in Figure 13, delivering the best performance across a broad TSR range.

7. Future Works

To build on this study, future research could broaden the TSR range for a more comprehensive understanding of optimal design parameters and validate the optimized turbine profiles through field tests to ensure real-world applicability. Investigating the material properties and structural resilience of the blades under various conditions would provide insights into their durability, while assessing environmental impacts and conducting a cost-benefit analysis would ensure the sustainability and economic viability of the optimized designs.

Acknowledgment

This work was carried out with the support of the Coordination for the Improvement of Higher Education Personnel– Brazil (CAPES) - Financing Code 001.

References

[1] A. Bianchini, F. Balduzzi, P. Bachant, G. Ferrara, and L. Ferrari, "Effectiveness of two-dimensional CFD simulations for Darrieus VAWTs: a combined numerical and experimental assessment," *Energy Conversion and Management*, vol. 136, pp. 318–328, Mar. 2017, doi: https://doi.org/10.1016/j.enconman.2017.01.026.

[2] L. Du, G. Ingram, and R. Dominy, "A review of H-Darrieus wind turbine aerodynamic research.," Journal of mechanical engineering science., vol. 233, no. 23–24, pp. 7590–7616, Dec. 2019, doi: https://doi.org/10.1177/0954406219885962.

[3] I. D. Brownstein, N. J. Wei, and J. O. Dabiri, "Aerodynamically Interacting Vertical-Axis Wind Turbines: Performance Enhancement and Three-Dimensional Flow," *Energies*, vol. 12, no. 14, p. 2724, Jul. 2019, doi: https://doi.org/10.3390/en12142724.

[4] M. Ghasemian, Z. N. Ashrafi, and A. Sedaghat, "A review on computational fluid dynamic simulation techniques for Darrieus vertical axis wind turbines," *Energy Conversion and Management*, vol. 149, pp. 87–100, Oct. 2017, doi: https://doi.org/10.1016/j.enconman.2017.07.016.

[5] N. Ma *et al.*, "Airfoil optimization to improve power performance of a high-solidity vertical axis wind turbine at a moderate tip speed ratio," *Energy*, vol. 150, pp. 236–252, May 2018, doi: https://doi.org/10.1016/j.energy.2018.02.115.

[6] Z. Zhang, D. Gao, J. Li, and X. Jia, "A New Method of Sectional Expression of Wind Turbine Airfoil Function," *Energies*, vol. 14, no. 21, p. 7309, Nov. 2021, doi: https://doi.org/10.3390/en14217309.

[7] S. Le Fouest and K. Mulleners, "The dynamic stall dilemma for vertical-axis wind turbines," Renewable Energy, Aug. 2022, doi: https://doi.org/10.1016/j.renene.2022.07.071.

[8] A.-J. Buchner, J. Soria, D. Honnery, and A. J. Smits, "Dynamic stall in vertical axis wind turbines: scaling and topological considerations," *Journal of Fluid Mechanics*, vol. 841, pp. 746–766, Feb. 2018, doi: https://doi.org/10.1017/jfm.2018.112.

[9] Z. Zhao *et al.*, "Variable Pitch Approach for Performance Improving of Straight-Bladed VAWT at Rated Tip Speed Ratio," *Applied Sciences*, vol. 8, no. 6, p. 957, Jun. 2018, doi: https://doi.org/10.3390/app8060957.

[10] C. Ma, Z. Yang, K. Jiao, Z. Liu, and Q. Du, "Multi-objective optimization of the centrifugal compressor impeller in 130 kW PEMFC through coupling SVM with NSGA -III algorithms," International Journal of Green Energy, vol. 18, no. 13, pp. 1383–1395, May 2021, doi: https://doi.org/10.1080/15435075.2021.1904942.

[11] D. C. Montgomery and G. C. Runger, *Applied statistics and probability for engineers*. Hoboken, Nj Wiley, 2018.

[12] A. Labijak-Kowalska and Miłosz Kadziński, "Exact and stochastic methods for robustness analysis in the context of Imprecise Data Envelopment Analysis," *Operational Research*, vol. 23, no. 1, Mar. 2023, doi: https://doi.org/10.1007/s12351-023-00755-z.

[13] S. R. Bistafa, "On the development of the Navier-Stokes equation by Navier," *Revista Brasileira de Ensino de Física*, vol. 40, no. 2, Nov. 2017, doi: https://doi.org/10.1590/1806-9126-rbef-2017-0239.

[14] I. Hashem and M. H. Mohamed, "Aerodynamic performance enhancements of H-rotor Darrieus wind turbine," *Energy*, vol. 142, pp. 531–545, Jan. 2018, doi: https://doi.org/10.1016/j.energy.2017.10.036

[15] A. Rezaeiha, I. Kalkman, and B. Blocken, "CFD simulation of a vertical axis wind turbine operating at a moderate tip speed ratio: Guidelines for minimum domain size and azimuthal increment," *Renewable Energy*, vol. 107, pp. 373–385, Jul. 2017, doi: https://doi.org/10.1016/j.renene.2017.02.006.

[16] P. A. C. Rocha, H. H. B. Rocha, F. O. M. Carneiro, M. E. V. da Silva, and C. F. de Andrade, "A case study on the calibration of the k–ω SST (shear stress transport) turbulence model for small scale wind turbines designed with cambered and symmetrical airfoils," Energy, vol. 97, pp. 144–150, Feb. 2016, doi: https://doi.org/10.1016/j.energy.2015.12.081.

[17] F. Balduzzi, A. Bianchini, R. Maleci, G. Ferrara, and L. Ferrari, "Critical issues in the CFD simulation of Darrieus wind turbines," *Renewable Energy*, vol. 85, pp. 419–435, Jan. 2016, doi: https://doi.org/10.1016/j.renene.2015.06.048.

[18] H. F. Lam and H. Y. Peng, "Study of wake characteristics of a vertical axis wind turbine by two- and three-dimensional computational fluid dynamics simulations," *Renewable Energy*, vol. 90, pp. 386–398, May 2016, doi: https://doi.org/10.1016/j.renene.2016.01.011.

[19] F. Trivellato and M. Raciti Castelli, "On the Courant–Friedrichs–Lewy criterion of rotating grids in 2D vertical-axis wind turbine analysis," *Renewable Energy*, vol. 62, pp. 53–62, Feb. 2014, doi: https://doi.org/10.1016/j.renene.2013.06.022.

[20] A. Rezaeiha, I. Kalkman, and B. Blocken, "Effect of pitch angle on power performance and aerodynamics of a vertical axis wind turbine," *Applied Energy*, vol. 197, pp. 132–150, Jul. 2017, doi: https://doi.org/10.1016/j.apenergy.2017.03.128.

[21] S. Salvadori, "Uncertainty Quantification in CFD: The Matrix of Knowledge," Springer eBooks, pp. 33–66, Jun. 2018, doi: https://doi.org/10.1007/978-3-319-92943-9_2.

[22] B. Belabes and M. Paraschivoiu, "Numerical study of the effect of turbulence intensity on VAWT performance," *Energy*, vol. 233, p. 121139, Oct. 2021, doi: https://doi.org/10.1016/j.energy.2021.121139.

[23] M. Raciti Castelli, A. Englaro, and E. Benini, "The Darrieus wind turbine: Proposal for a new performance prediction model based on CFD," *Energy*, vol. 36, no. 8, pp. 4919–4934, Aug. 2011, doi: https://doi.org/10.1016/j.energy.2011.05.036.

[24] Z. Zhang, D. Gao, J. Li, and X. Jia, "A New Method of Sectional Expression of Wind Turbine Airfoil Function," *Energies*, vol. 14, no. 21, p. 7309, Nov. 2021, doi: https://doi.org/10.3390/en14217309.

[25] L. Zhang, Y. Liang, X. Liu, and J. Guo, "Effect of blade pitch angle on aerodynamic performance of straight-bladed vertical axis wind turbine," *Journal of Central South University*, vol. 21, no. 4, pp. 1417–1427, Apr. 2014, doi: https://doi.org/10.1007/s11771-014-2080-7.

[26] H. He, L. Yi, and J. Peng, "Combinatorial Optimization Algorithm of MIGA and NLPQL for a Plug-in Hybrid Electric Bus Parameters Optimization," Energy Procedia, vol. 105, pp. 2460–2465, May 2017, doi: https://doi.org/10.1016/j.egypro.2017.03.708.

[27] P. Raska and Z. Ulrych, "Comparison of Modified Downhill Simplex and Differential Evolution with other Selected Optimization Methods Used for Discrete Event Simulation Models," Procedia Engineering, vol. 100, pp. 807–815, 2015, doi: https://doi.org/10.1016/j.proeng.2015.01.435.

[28] P. F. S. Trentin, P. H. B. de B. Martinez, G. B. dos Santos, E. E. Gasparin, and L. O. Salviano, "Screening analysis and unconstrained optimization of a small-scale vertical axis wind turbine," *Energy*, vol. 240, p. 122782, Feb. 2022, doi: https://doi.org/10.1016/j.energy.2021.122782.